Lateral Growth of Uniformly Thin Gold Nanosheet Facilitated by Two-dimensional Precursor Supply

Koki Sasaki, Tsuyoshi Okue, Takuto Nakai, Yoshiaki Uchida,* and Norikazu Nishiyama

Graduate School of Engineering Science, Osaka University, 1-3 Machikaneyama-cho, Toyonaka, Osaka 560-8531, Japan

Supporting Information Placeholder

ABSTRACT: Nanosheets of highly symmetric materials with a face-centered cubic lattice like gold have been synthesized by adsorbing the precursors on a flat surface, whose chemical specificity induces the anisotropy of growth rates. Here, we have succeeded in the fabrication of gold nanosheets in hydrophilic space inside highly-separated bilayers, which work as two-dimensional hydrophilic reactors, in a hyperswollen lamellar liquid crystalline phase of an amphiphile solution. One of the physical properties, amphiphilicity, confines the ingredients therein. The nanosheets can only grow in the in-plane direction due to inhibition of the out-of-plane growth rather than the anisotropy of growth rates probably. Thus, the synthesis can be accelerated; the particles can be completed within 15 minutes. As not relying on chemical specificity, silver nanosheets could also be synthesized in the same way. The suspension of gold and silver nanosheets without any amphiphiles could be obtained, and the solvent is replaceable. We found that the obtained gold nanosheets' width is proportional to the Reynolds number of the solution because the bilayer's area in the hyperswollen lamellar phase depends on shear stress. They imply that the areas of gold nanosheets depend on bilayers' areas, and it can be controlled by changing the Reynolds number. This method could be widely used to continuously obtain large-area nanosheets of various materials in a roll-to-roll manufacturing process.

Introduction

Crystals with cubic lattices intrinsically grow in three dimensions; the cubic lattice system is also called an isometric system. Their high-symmetry structures contribute to the high ductility of face-centered cubic (fcc) metals and the absence of anisotropy like birefringence and ferroic properties. Symmetry breaking of their crystal shapes leads to a variety of anisotropic properties. Nanosized fcc metals with shape anisotropy show unique properties: e.g., two plasmon bands of silver (Ag) nanorods[1] and the high catalytic activity.[2] Among nanosized materials, nanosheets have safety, dispersibility, and nanosize effects together. The ductility allows the fcc metals to be thinned down to 100 nm using top-down rolling and beating methods.[3]

Bottom-up methods can fabricate thinner nanosheets than top-down methods. Since they can decrease the thickness down to nanometer order, the obtained nanosheets frequently exhibit the various nanosize effects. Anisotropic growth of materials with cubic lattices occurs in some specific circumstances; the growth inhibition of a certain crystal plane[4-6] and the priority growth on a template[7-10] can give fcc metal nanosheets with several nm thicknesses. Generally, chemical specificity drives the anisotropic growth. For example, gold nanosheets (AuNSs) with high conductivity,[10] high catalytic performance,[11] and unique surface plasmon polariton features[12] have been synthesized at liquid-liquid, gas-liquid, solid-liquid, and gas-solid interfaces. They can be applied to electronics,[13] biosensors,[14] and plasmonics.[12] These are based on the difference in the growth rates between a certain dimension and the other dimensions. The excessive increase of the reaction rates often reduces the particles' shape anisotropy in the nanosheet synthesis due to the three-dimensional precursor supply, as shown in Figure 1a.[8,9,15,16]

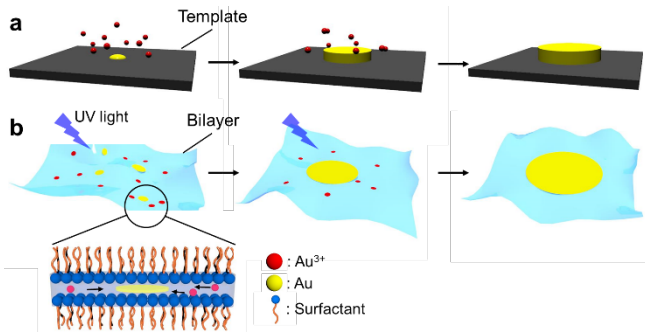

Figure 1. Schematic illustration of the growth mechanism of AuNSs. (a) Conventional methods three-dimensionally supply precursors on two-dimensional templates. (b) The present method two-dimensionally confines precursors in a bilayer.

Bilayers in hyperswollen lyotropic lamellar (HL) phases of dilute aqueous amphiphile solutions confine hydrophobic molecules in several nm thick two-dimensional (2-D) space, and they keep several hundred nm intervals between two adjacent bilayers.[17] The confined hydrophobic molecules react to give hydrophobic nanosheets;[18] this synthesis method is named 'two-dimensional reactor in amphiphilic phases (TRAP) method.' The TRAP method can synthesize nanosheets of metal-organic frameworks (MOFs)[19,20] and amorphous polymers[18] because the hydrophobic precursors are physically trapped in the hydrophobic TRAPs sterically repelling with each other.[21] We guess that the 2-D precursor supply promotes only lateral growth of any materials, as shown in Figure 1b. The fcc metal nanosheets could also grow in a hydrophilic TRAP, which has been unexplored. The new TRAP method could be applied to other hydrophilic materials such as fcc metal oxides, organometallic compounds, and other cubic crystalline materials.

Here, we report the fuss-free synthesis of uniformly thin AuNSs within 15 minutes using an unprecedented hydrophilic TRAP method. We discuss the growth mechanism of the AuNSs using atomic force microscopy (AFM) and X-ray diffraction (XRD) measurements. Based on the conceivable mechanism, we propose

the lateral size control method for AuNSs that focuses on the size of the TRAPs. Moreover, we synthesized Ag nanosheets (AgNSs) as another fcc metal example to demonstrate the method's universality.

Materials and Methods

Materials and equipment. Decane, 1-pentanol, p-octylbenzenesulfonate (OBS), ethanol, and tetrachloroauric (III) acid ($HAuCl_4$) were purchased from Wako Pure Chemical Industries Co. The water used was obtained from a water purifier (Direct-Q UV) with a resistivity of 18.2 MΩ cm. The UV lamp (AT250S) was purchased from ARK Technologies, Inc.

Synthesis of AuNSs in the bilayer consisted of OBS. AuNSs were synthesized in the hyperswollen lyotropic lamellar (HL) phases of the decane solutions of OBS (0.95 wt%), 1-pentanol (8.4 wt%) and deionized water (1.1 wt%). $HAuCl_4$ was added to the decane solution at various concentrations (c, 2.5×10^{-2} – 1.0×10^{-1} wt%). The solution was poured into the vessel (Φ, 15 – 60 mm of inner diameter) up to a height of 30 mm, and irradiated with UV light of various intensities (I, 0.36 – 4.1 W) from 35 mm above the liquid surface for various reaction times (t_r, 5 – 15 minutes) with stirring (200 rpm). The final products were centrifuged at 11,000 rpm for 1 h and washed three times with methanol.

Synthesis of gold fine particles. Gold (Au) fine particles were synthesized in the solution consisted of decane (90.4 wt%), 1-pentanol (8.50 wt%), deionized water (1.09 wt%), and $HAuCl_4$ (5.0×10^{-2} wt%). The solution was poured into the vessel (60 mm of inner diameter) up to a height of 30 mm, and irradiated with UV light with 1.53 W from 35 mm above the liquid surface for 15 minutes with stirring (200 rpm). The final products were centrifuged at 11,000 rpm for 1 h and washed three times with methanol.

Synthesis of AuNSs in the bilayer consisted of Brij L4. AuNSs were synthesized in the hyperswollen lyotropic lamellar (HL) phases of the decane solution of Brij L4 (7.0 wt%), deionized water (1.6 wt%), and $HAuCl_4$ (5.0×10^{-2} wt%). The solution was poured into the vessel (Φ, 15-60 mm of inner diameter) up to a height of 30 mm, and irradiated with UV light with 1.53 W from 35 mm above the liquid surface for various reaction times (t_r, 5-15 minutes) with stirring (200 rpm). The final products were centrifuged at 11,000 rpm for 1 h and washed three times with methanol.

Synthesis of AgNSs. We prepared the decane solution of OBS (0.94 wt%), 1-pentanol (8.31 wt%), deionized water (1.1 wt%), and silver(I) nitrate (1.0×10^{-1} wt%), and that of OBS (0.93 wt%), decane (89.6 wt%), 1-pentanol (8.3 wt%), deionized water (1.1 wt%) and sodium hydroxide (NaOH) (4.0×10^{-2} wt%). The solution containing silver(I) nitrate was purred into the vessel (60 mm of inner diameter) up to a height of 15 mm, and the solution containing NaOH was purred into the same vessel up to a height of 30 mm. The mixture was irradiated with UV light with 1.53 W from 35 mm above the liquid surface for 15 minutes with stirring (200 rpm). The final products were centrifuged at 11,000 rpm for 1 h and washed three times each with methanol and ethanol.

Synthesis of silver fine particles. We prepared the decane solution of 1 - pentanol (8.39 wt%), deionized water (1.1 wt%), and silver(I) nitrate (1.0×10^{-1} wt%), and that of 1-pentanol (8.4 wt%), deionized water (1.1 wt%) and sodium hydroxide (NaOH) (4.0×10^{-2} wt%). The solution containing silver(I) nitrate was purred into the vessel (60 mm of inner diameter) up to a height of 15 mm, and the solution containing NaOH was purred into the same vessel up to a height of 30 mm. The mixture was irradiated with UV light with 1.53 W from 35 mm above the liquid surface for 15 minutes with stirring (200 rpm). The final products were centrifuged at 11,000 rpm for 1 h and washed three times each with methanol and ethanol.

Results and Discussion

The experimental setup for the synthesis of AuNSs is shown in Figure 2. The decane solutions of tetrachloroauric (III) acid ($HAuCl_4$) with various concentrations (c, 2.5×10^{-2} – 1.0×10^{-1} wt%) were poured into the vessels containing an agitator with various lengths (L, 15 – 60 mm), and irradiated with UV light, whose spectrum is shown in Figure S1, with various intensities (I, 0.36 – 4.1 W) for various reaction times (t_r, 5 – 15 minutes) with stirring (200 rpm). We fixed the distances between the UV lamp and the solution surface and the solution depth to be 35 mm and 30 mm, respectively, to keep the UV light energy constant. The decane solutions of sodium *p*-octylbenzenesulfonate (OBS), 1-pentanol, and water have been reported to exhibit HL phases.[22] The hydrophilic TRAP method needs to check if the amphiphile solution exhibits the HL phase, even with ingredients addition. We could observe the birefringence of the solutions in crossed Nicols from any direction using a polarizing film wrapped around the vessel, as shown in Figure 2c.[23] The photograph of the decane solutions surrounded by a polarizing film shows a colorful texture typical of HL phases, as shown in Figure 3a. When we added $HAuCl_4$ (5.0×10^{-2} wt%) as one of the ingredients to the decane solution, this solution maintains HL phases, as shown in Figure 3b. The hydrophilic bilayers are likely to trap $HAuCl_4$ stably. After the irradiation with UV light of 4.1 W for 5 minutes, the reaction mixture's color changed from yellow to purple, as shown in Figure S2. It suggests that the particles grew. The reaction mixture still maintained the HL phase, as shown in Figure 3c. It implies that the formation of Au particles does not disturb the HL phase.

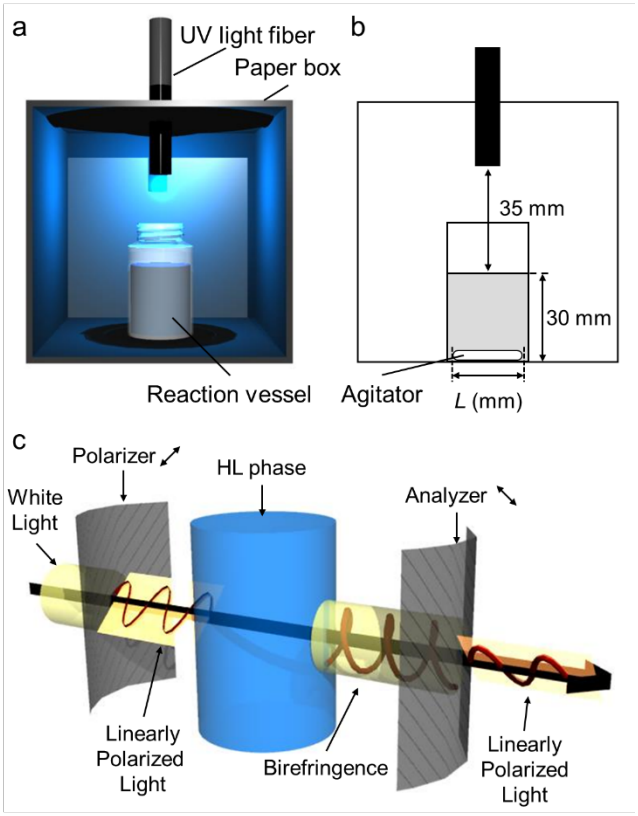

Figure 2. Schematic illustration of the experimental setup. a) Cartoon and b) scheme of the experimental setup. c) Optical system to observe the birefringence of the reaction mixture using a polarizing film wrapped around a container while tilted 45 degrees.

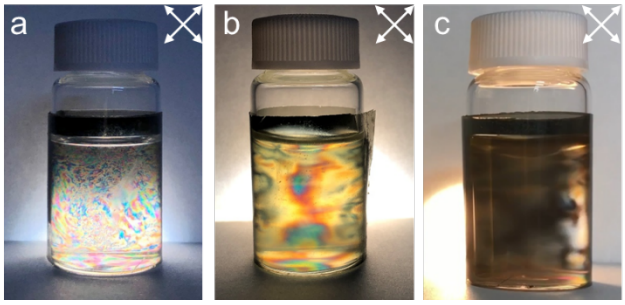

Figure 3. Polarized photographs of hyperswollen lyotropic lamellar phases. (a) Decane solution of OBS (0.95 wt%), 1-pentanol (8.4 wt%), water (1.1 wt%). The reaction mixture for AuNSs synthesis (b) before reaction and (c) after reaction showed liquid crystalline textures.

The reaction mixture was centrifuged at 11,000 rpm for 1 h, and the precipitate was washed three times with methanol to give a dark blue powder (90% yield). The XRD pattern of the dark blue powder showed the same peaks and intensity ratios as the Au fine particles with a more than 100 nm diameter, as shown in Figure 4a. It implies that the obtained dark blue powder seems to be metallic Au, and the growth inhibition of some certain crystal planes does not occur in the bilayer. The particle size distributions estimated from dynamic light scattering (DLS) measurements of the products look sharp, as shown in Figure 4b. The TEM photographs indicate the samples are nanosheets, as shown in Figures S4a-c. The selected area electron diffraction pattern gives evidence of the crystallinity of the sample, as shown in Figure S4d. All the products are likely to be mono-dispersed. The horizontal width and thickness of the products measured by AFM are 1500 ± 560 nm and 2.18 ± 0.50 nm, respectively, as shown in Figure 4c. These results indicate that the products are AuNSs. We have to figure out the growth mechanism.

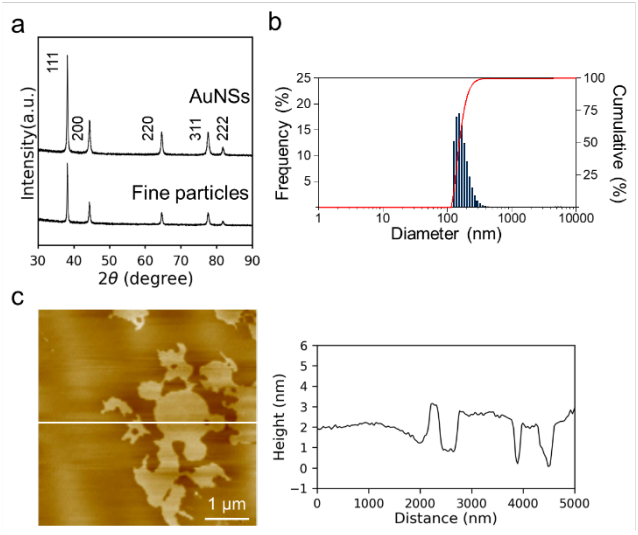

Figure 4. Characterization of AuNSs. (a) X-ray diffraction pattern of the AuNSs. (b) The DLS analysis of AuNSs. (c) AFM photograph and cross-section of one of the synthesized AuNSs.

We focus on the lateral fusion of the AuNSs shown in Figure 4c. The TEM photograph also gives evidence of the fusion, as shown in Figure S4a. The edge of most AuNSs is curved, and AuNSs rarely have corners shown in Figure S4b. The full width at half maximum (FWHM) of each of the XRD peaks for the AuNSs was broader than that of the large particles, as shown in Table S1. The Williamson-Hall plots shown in Figure S5 indicate that the crystallite size of the AuNSs is smaller than that of Au fine particles.[24] The uniformly nanosized Au particles are likely to fuse laterally in the confined thin 2-D reaction field of the HL phase. These results imply that the amphiphilic molecules do not protect the surfaces of the AuNSs.

The scanning electron microscope-energy dispersive X-ray spectrometry (SEM-EDX) of the AuNSs did not detect any sulfur elements, as shown in Figure S6. The amphiphile OBS should not protect that the surface of the AuNSs. Interestingly, the suspension solvent is replaceable with various solvents like hexane, diethyl ether, ethyl acetate, toluene, chloroform, tetrahydrofuran (THF), and acetone, as shown in Figures S7-S9. The surface of the AuNSs seems stable because the physically-confined nanosized Au particles are randomly fused. The physical confinement probably decides the thickness of the AuNSs. However, we have not understood the factors that decide the width of the AuNSs, yet.

The growth of particles by photochemical reactions generally depends on the precursor's concentration (c) and the light intensity (I).[8] Of course, because the width of the AuNSs increases with t_r, as shown in Figure S10, we discuss the dependence of the convergent width of the AuNSs on c and I. The width and thickness of the AuNSs for each of several synthetic conditions were measured through AFM, as shown in Table S2, and the size distribution of these AuNSs were estimated from DLS measurements, as shown in Figure S11. The thicknesses of the AuNSs were likely to be independent of I between 1.53 and 4.10 W. Although the thickness of the AuNSs obtained with the UV irradiation of 0.36 W is thicker than the others, the AuNSs was thinner than 4 nm as long as the reaction mixtures exhibited HL phases, as shown in Figure S12. The AuNSs probably grow thicker when the reaction rate is lower than the diffusion rate. We could consider the diffusion to be 2-D as long as the reaction rate is higher than the diffusion rate. In the range of the reaction rate where quasi-2-D diffusion is valid, the volume of the AuNSs linearly increased as c increased, though the dependence of the width and thickness of the AuNSs on c was ambiguous, as shown in Figures S13 and S14. The volume does not look proportional to c, and therefore, the nucleation seems to depend on c. It implies that multiple AuNSs grow in each bilayer, and therefore, bilayer width could be one of the factors deciding the width of the AuNSs.

We have not had the information on the bilayer width. The width of AuNSs could be proportional to the square root of bilayer area, A, which linearly depends on the excess internal elastic stress (σ_i),[25]

$$\sigma_i = \sigma - \eta\dot{\gamma},$$

where $\dot{\gamma}$ is the stirring rate, σ is the total shear stress, and η is the solution's viscosity; however, the relation between σ and $\dot{\gamma}$ is not clear in hyperswollen lamellar phases. The mechanics of such a viscous fluid generally depends on inertial and viscous forces. The controllable parameters are $\dot{\gamma}$ and L. When $\dot{\gamma}$ increases, the solution surface deforms, and the distance between the UV lamp and the solution surface becomes not uniform. It would further complicate the situation. Therefore, we measured the dependence of the convergent width of AuNSs on L. The AuNSs width seems proportional to L^2, as shown in Figure 5. It suggests that the bilayer's expansion causes the increase of the AuNSs width because L^2 is proportional to Reynolds number as listed in Table S3, which is the ratio of inertial force to viscous force.[26] Reynolds number should be useful as the indicator for controlling the AuNSs' width and scale-up using continuous flow reactors. Besides, AuNSs could be synthesized in the bilayers in the HL phase of a decane solution of non-ionic amphiphile Brij L4 were smaller than those obtained from the ionic OBS solutions, as shown in Figures S15-S18 and Table S4. It is likely because the bilayers' width was smaller than those obtained from the OBS solution. It is consistent with the general trends that ionic amphiphiles generally make more stable

lamellar structures than non-ionic amphiphiles. We have to confirm the universality of the hydrophilic TRAP method.

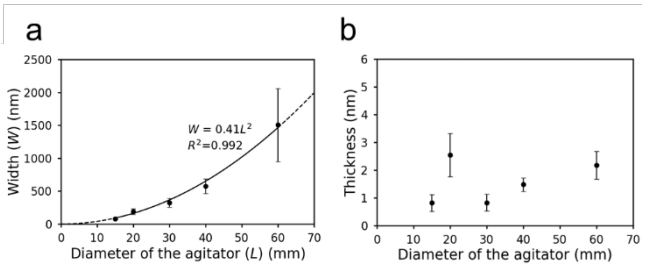

Figure 5. Dependence of the convergent AuNSs size on *L*. (a) Width and (b) thickness of the AuNSs.

We synthesized AgNSs as another example of nanosheets of fcc metals. The photoreduction reaction of silver(I) nitrate in the same experimental setup as that for AuNSs gave a black powder, as shown in Figures S19 and S20. The XRD pattern of the obtained powder shows the same peaks as the Ag fine particles, as shown in Figure 6a. Therefore, the obtained powder seems to be metallic Ag. The size distribution estimated from the DLS measurement of the obtained powder looks as sharp as that of AuNSs, as shown in Figure 6b. The TEM photographs indicate the samples are nanosheets and the selected area electron diffraction pattern gives evidence of the crystallinity of the sample, as shown in Figure S21. The horizontal width and thickness of the products measured through AFM were 1000 ± 500 nm and 1.55 ± 0.82 nm, respectively, as shown in Figure 6c. These results indicate that the TRAP method enables us to synthesize the nanosheets of various fcc metals.

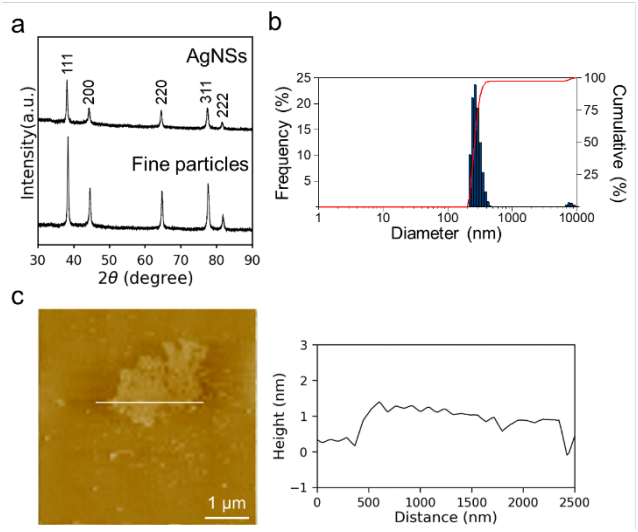

Figure 6. Characterization of AgNSs: (a) X-ray diffraction pattern of the AgNSs; (b) The DLS analysis of AgNSs; (c) AFM photograph and cross-section of one of the synthesized AgNSs.

Conclusion

In summary, uniformly thin AuNSs with a few nm thicknesses have been successfully synthesized within 15 minutes using the hydrophilic TRAP method. The nanosheets only show in-plane growth due to the 2-D precursor supply. The AuNSs' width seems proportional to the Reynolds number of the solution because the bilayer area in the hyperswollen lamellar phase depends on shear stress. The hydrophilic TRAP method could also be applied for Ag with fcc lattice as the fuss-free synthesis method because the precursors are accumulated due to rather physical confinement than chemical specificity. This method can apply to nanosheet composed of metals, metal oxides, organometallic complexes, and organic crystals. Reynolds number is useful as the indicator to control the nanosheets' width; this method will continuously obtain large-area nanosheets in a roll-to-roll manufacturing process in the future.

ASSOCIATED CONTENT

Supporting Information

The Supporting Information is available free of charge on the ACS Publications website.

Characterization methods, spectrum of the light source, photographs and polarized photographs of reaction mixture, TEM photograph, XRD peak position and FWHM, Williamson-Hall plots, SEM-EDX spectra, photographs of suspensions of AuNSs with various solvents, size distributions, and AFM photographs (PDF)

AUTHOR INFORMATION

Corresponding Author

*yuchida@cheng.es.osaka-u.ac.jp

Notes

The authors declare no competing financial interest.

ACKNOWLEDGMENT

A part of this work was supported by "Advanced Characterization Nanotechnology Platform, Nanotechnology Platform Program of the Ministry of Education, Culture, Sports, Science and Technology (MEXT), Japan, Grant Number JPMXP09A20OS0024 at the Research Center for Ultra-High Voltage Electron Microscopy (Nanotechnology Open Facilities) in Osaka University. The authors thank Prof. T. Hirai and Prof. Y. Shiraishi for their help with the use of the dynamic light scattering. The authors thank Prof. Y. Shiraishi and Prof. T. Mitsudome for helpful advice. This work was supported in part by the Japan Science and Technology Agency (JST) "Precursory Research for Embryonic Science and Technology (PRESTO)" for a project of "Molecular technology and creation of new function", and JSPS KAKENHI Grant Number JP20H05161.

REFERENCES

(1) Murphy, C. J.; Sau, T. K.; Gole, A.; Orendorff, C. J. Surfactant-Directed Synthesis and Optical Properties of One-Dimensional Plasmonic Metallic Nanostructures. *MRS Bulletin*, **2005**, *30*, 349–355.
(2) Jiji, S. G.; Gopchandran, K. G. Shape dependent catalytic activity of unsupported gold nanostructures for the fast reduction of 4-nitroaniline. *Colloid Interface Sci. Commun.*, **2019**, *29*, 9–16.
(3) Gupta, C. K.; Rohilla, Aman; Singh, R. P.; Singh, G; and Chamoli, S. K. Novel technique of making thin target foil of high density material via rolling method. *AIP Conf. Proc.*, **2018**, *1962*, 030013.
(4) Huang, X. Q.; Tang, S. H.; Mu, X. L.; Dai, Y.; Chen, G. X.; Zhou, Z. Y.; Ruan, F. X.; Yang, Z. L.; Zheng, N. F. Freestanding palladium nanosheets with plasmonic and catalytic properties. *Nat. Nanotechnol.*, **2011**, *6*, 28–32.
(5) Duan, H. H.; Yan, N.; Yu, R.; Chang, C. R.; Zhou, G.; Hu, H. S.; Rong, H. P.; Niu, Z. Q.; Mao, J. J.; Asakura, H.; Tanaka, T.; Dyson, P. J.; Li, J.; Li, Y. D. Ultrathin rhodium nanosheets. *Nat. Commun.*, **2014**, *5*, 3093.
(6) Zhao, L.; Xu, C. F.; Su, H. F.; Liang, J. H.; Lin, S. C.; Gu, L.; Wang, X. L.; Chen, M.; Zheng, N. F. Single-Crystalline Rhodium Nanosheets with Atomic Thickness. *Adv. Sci.*, **2015**, *2*, 1500100.
(7) Huang, X.; Li, S.; Huang, Y.; Wu, S.; Zhou, X.; Li, S.; Gan, C. L.; Boey, F.; Mirkin, C. A.; Zhang, H. Synthesis of hexagonal close-packed gold nanostructures. *Nat. Comm.*, **2011**, *2*, 292.
(8) Qin, H. L.; Wang, D.; Huang, Z. L.; Wu, D. M.; Zeng, Z. C.; Ren, B.; Xu, K.; Jin, J. Thickness-Controlled Synthesis of Ultrathin Au Sheets and Surface Plasmonic Property. *J. Am. Chem. Soc.*, **2013**, *135*, 12544–12547.
(9) Zhou, M.; Lin, M.; Chen, L.; Wang, Y.; Guo, X.; Peng, L.; Guo, X.; Dinga, W. Thickness-dependent SERS activities of gold nanosheets

controllably synthesized via photochemical reduction in lamellar liquid crystals. *Chem. Commun.*, **2015**, *51*, 5116–5119
(10) Yue, Y.; Norikane, Y. Gold clay from self-assembly of 2D microscale nanosheets. *Nat. Commun*., **2020**, *10*, 1–9.
(11) Ye, S.; Brown, A. P.; Stammers, A. C.; Thomson, N. H.; Wen, J.; Roach, L.; Bushby, R. J.; Coletta, P. L.; Critchley, K.; Connell, S. D.; Markham, A. F.; Brydson, R.; Evans, S. D. Sub-Nanometer Thick Gold Nanosheets as Highly Efficient Catalysts. *Adv. Sci*., **2019**, *6*, 1900911.
(12) Major, T. A.; Devadas, M. S.; Lo, S. S.; Hartland, G. V. Optical and Dynamical Properties of Chemically Synthesized Gold Nanoplates. *J. Phys. Chem. C,* **2013**, *117*, 1447–1452.
(13) Moon, G. D.; Lim, G.-H.; Song, J. H.; Shin, M.; Yu, T.; Lim, B; Jeong, U. Highly Stretchable Patterned Gold Electrodes Made of Au Nanosheets. *Adv. Mater.*, **2013**, *25*, 2707–2712.
(14) Lim, G.-H.; Lee, N.-E.; Lim, B. Highly sensitive, tunable, and durable gold nanosheet strain sensors for human motion detection. *J. Mater. Chem. C*, **2016**, *4*, 5642–5647.
(15) Momeni, S.; Safavi, A.; Ahmadib, R.; Nabipoura, I. Gold nanosheets synthesized with red marine alga Actinotrichia fragilis as efficient electrocatalysts toward formic acid oxidation. *RSC Adv.*, **2016**, *6*, 75152–75161.
(16) He, S.; Hai, J.; Li, T.; Liu, S.; Chen, F.; Wang. B. Photochemical strategies for the green synthesis of ultrathin Au nanosheets using photoinduced free radical generation and their catalytic properties. *Nanoscale*, **2018**, *10*, 18805–18811.
(17) Strey, R.; Schomacker, R. Dilute Lamellar and L_3 Phases in the Binary Water-$C_{12}E_5$ System. *J. Chem. Soc. Faraday Trans.*, **1990**, *86*, 2253-2261.
(18) Uchida, Y.; Nishizawa, T.; Omiya, T.; Hirota, Y.; Nishiyama, N. Nanosheet Formation in Hyperswollen Lyotropic Lamellar Phases. *J. Am. Chem. Soc.,* **2016**, *4*, 1103–1105.
(19) Omiya, T.; Sasaki, K.; Uchida, Y.; Nishiyama, N. Nanosheet Synthesis of Metal Organic Frameworks in a Sandwich like Reaction Field for Enhanced Gate-Opening Pressures. *ACS Appl. Nano Mater*., **2018**, *1*, 3779–3784.
(20) Omiya, T.; Sasaki, K.; Uchida, Y.; Nishiyama, N. Synthesis of MOF Nanosheets in Hyperswollen Lyotropic Lamellar Phase. *Mol. Cryst. Liq. Cryst.*, Taylor & Francis, **2019**, *684*, 1–6.
(21) Yamamoto, J.; Tanaka, H. Dynamic control of the photonic smectic order of membranes. *Nat. Mater.*, **2005**, *4*, 75–80.
(22) Larche, F. C.; Appell, J.; Porte, G.; Bassereau, P.; Marignan, J. The Swelling of a Lamellar Lyotropic Liquid Crystal by an Alkane. J. *Phys. Rev. Lett.*, **1986**, *56*, 1700–1703.
(23) Miyamoto, N.; Nakato, T. Liquid Crystalline Nature of $K_4Nb_6O_{17}$ Nanosheet Sols and Their Macroscopic Alignment. *Adv. Mater*., **2002**, *14*, 1267–1270.
(24) Madhavi, J. Comparison of average crystallite size by X-ray peak broadening and Williamson–Hall and size–strain plots for VO^{2+} doped ZnS/CdS composite nanopowder. *SN Appl. Sci.*, **2019**, *1*, 1509.
(25) Yamamoto, J.; Tanaka, H. Shear Effects on Layer Undulation Fluctuations of a Hyperswollen Lamellar Phase. *Phys. Rev. Lett.*, **1995**, *74*, 932–935.
(26) Welty, J. R.; Wicks, C. E.; Rorrer, G. L.; Wilson, R. E. Fundamentals of Momentum, Heat and Mass Transfer, 5th ed., John Wiley & Sons, Inc., New York, **2007**.

Lateral Growth of Uniformly Thin Gold Nanosheet Facilitated by Two-dimensional Precursor Supply

Koki Sasaki, Tsuyoshi Okue, Takuto Nakai, Yoshiaki Uchida,* and Norikazu Nishiyama